Thermal stability and energy-band alignment of nitrogen-incorporated ZrO_2 films on Si(100)

L. Q. Zhu,[a] L. D. Zhang, G. H. Li, G. He, and M. Liu
Key Laboratory of Materials Physics, Anhui Key Laboratory of Nanomaterials and Nanostructure, Institute of Solid State Physics, Chinese Academy of Science, Hefei 230031, People's Republic of China

Q. Fang
Electronic & Electrical Engineering and London Centre for Nanotechnology, University College London, Torrington Place, London WCIE 7JE, United Kingdom

(Received 21 January 2006; accepted 9 May 2006; published online 6 June 2006)

Thermal stability and energy-band alignment of ZrO_xN_y films on Si are investigated using x-ray photoelectron spectroscopy and spectroscopy elliposometry (SE). The results show that the Zr–N bonds in as-oxidized ZrO_xN_y films are thermally unstable, while the N–O bonds in ZrO_xN_y matrix are stable even at high annealing temperature of 900 °C. Optical properties are also analyzed based on the SE fitting results. The slight blueshift in the absorption edge indicates the increased band gap from 3.9 to 5.1 eV after the additional annealing. Based on the valence-band spectrum results, zero-field energy-band alignments for ZrO_xN_y/Si and $ZrO_xN_y/SiO_2/Si$ stacks are extracted. © *2006 American Institute of Physics*. [DOI: 10.1063/1.2209882]

With the continual scaling down of feature sizes in complementary metal-oxide semiconductor (CMOS) devices, the conventionally used SiO_2 gate dielectric thickness has been pushed below 15 Å, which causes reduced dielectric reliability and significant gate leakage current.[1,2] As a result, research has focused recently on investigating high-*k* gate dielectrics, which may potentially replace SiO_2 in advanced CMOS technologies.[1] As a conventional high-*k* candidate, ZrO_2 has been received considerable attention.[3–8] However, ZrO_2 is a poor barrier to oxygen diffusion, which causes the uncontrolled low-*k* interfacial layer growth between ZrO_2 and Si substrate during high temperature annealing processing[9,10] and, hence, imposes serious concern to equivalent oxide thickness (EOT) scalability. Many reports show that nitrogen incorporated high-*k* oxides have increased crystallization temperature and decreased current leakage[11–14] because of the reduction in transition-metal coordination. Furthermore the presence of N in high-*k* oxides also reduces oxygen diffusion and impurities penetration through high-*k* oxides.[15,16] However, there are relatively few reports on the optical properties and electronic structure of ZrO_xN_y on Si in relation to annealing temperature. In this letter, we focus on the thermal stability and optical properties, as well as valence- and conduction-band offsets of ZrO_xN_y films on Si.

The ZrO_xN_y films were prepared by two subsequent procedures. Firstly, the targeted ZrN_x films were deposited on Si(100) substrates (*n* type, $\rho=1-10\ \Omega$ cm) by radio frequency (rf) sputtering of Zr target (99.99%) in Ar/N_2 ambient. Secondly, the ZrN_x films were subjected to an *ex situ* thermal oxidation in O_2/N_2 ambient ($O_2=2$ SCCM and $N_2=98$ SCCM) for 5 min at 500 °C. To evaluate the oxides response to the additional high temperature annealing, the as-prepared ZrO_xN_y films were subjected to a postoxidization annealing in O_2/N_2 ambient at 800 and 900 °C for 5 min. VG ESCALAB MK II x-ray photoelectron spectroscopy (XPS) was used to study the chemical bond and chemical composition of the ZrO_xN_y films. *Ex situ* spectroscopic phase-modulated ellipsometry (model UVISE JOBIN-YVON) has been employed to investigate the optical properties of ZrO_xN_y.

Figure 1 shows the Zr_{3d} portion and N_{1s} portion of the XPS signal. XPS analysis shows a slight higher Zr_{3d} binding energy in the as-deposited ZrN_x films than that of the standard Zr–N bond (not shown here) because the residual oxygen in the deposition chamber always exists during the Zr sputtering. In Fig. 1(a), there is a doublet corresponding to $3d_{5/2}$ and $3d_{3/2}$ features at 181.8 and 184.1 eV for as-oxidized sample. After annealing at high temperatures, the Zr_{3d} peaks show a slight blueshift and stabilize at 182.2 and 184.6 eV for $3d_{5/2}$ and $3d_{3/2}$ features, respectively. In Fig. 1(b), N_{1s} spectrum from normal ZrN_x and as-oxidized sample exhibits two peaks at around 395.5 and 402.6 eV, whereas only peaks at 402.6 eV are found for the annealed ones. The core level peak located at 395.5 eV corresponds to the atomic nitrogen of Zr–N bonds, while that at 402.6 eV to the N–O bonds. Similar peaks are also found in Hf–N bonds at 396 eV.[17] Since there is no any N_{1s} peak at around 402.6 eV for ZrO_2 system in the energy range of 392 –408 eV [as shown in the inset of Fig. 1(b)], we can conclude that the peaks at 402.6 eV are related to ZrO_xN_y matrix. According to Pauling theory,[18] ionicity in a single bond increases with the difference in values of electron nega-

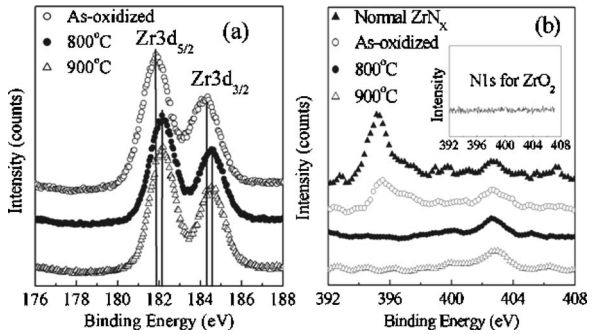

FIG. 1. XPS core level spectra of Zr_{3d} and N_{1s} for ZrO_xN_y films: (a) core level spectra of Zr_{3d} and (b) core level spectra of N_{1s}. The inset in (b) shows the XPS spectrum of ZrO_2 in the energy range of 392–408 eV. There is no observable N_{1s} peak, indicating no nitrogen adsorbed in ZrO_2 films.

[a]Electronic mail: qzhuli2003@yahoo.com.cn

TABLE I. ZrO_xN_y spectroscopic ellipsometric fitting results. sr represents the SE surface roughness of ZrO_xN_y films and rms represents the AFM root-mean-square surface roughness.

Temperature (°C)	As-oxidized	800 °C	900 °C
AFM rms (nm)	0.4	0.5	0.4
SE sr (nm)	0.8	1.0	0.8
ZrO_xN_y thickness (nm)	14.3	14.6	15.2
Interfacial layer (nm)	···	1.1	2.6
χ^2	2.1	2.0	1.4
E_g (eV)	3.9	5.1	5.1

tivity between two elements belong to this bond. Since the electronegativity of oxygen is larger than that of nitrogen (3.5 vs 3.0), the Zr–O bond involves a larger charge transfer than that in the Zr–N bond.[19] In our case, nitrogen atoms substitute the oxygen sites in the lattice of ZrO_2 crystal for as-oxidized ZrO_xN_y, which contributes to the decrease in ionicity and then the lower bonding energy for Zr_{3d}. After the additional high temperature annealing, oxygen oxidizes nitrogen sites in Zr–N bonds, resulting in the slight increase in Zr_{3d} binding energy, similar to that of Hf–N bonds.[16] However, there are no significant changes in N_{1s} peaks at 402.6 eV, indicating the stabilized Zr–O–N bonds even for high annealing temperature at 900 °C. Using standard sensitivity factors for O_{1s}, N_{1s}, and Zr_{3d}, the average nitrogen composition is determined to be 10.5 at. % for the normal ZrN_x film, 7.4 at. % for as-oxidized films, and 4.2 and 4.3 at. % for the annealed ones at 800 and 900 °C, respectively.

As a useful and nondestructive technique, spectroscopic ellipsometry (SE) has been employed to investigate the optical characteristics of ZrO_xN_y films as a function of annealing temperature. A simple two-layer optical model on silicon has been established for simulating the as-oxidized ZrO_xN_y films: homogeneous ZrO_xN_y films and surface rough layer which was assumed to be consisted of voids and ZrO_xN_y based on the Bruggeman effective medium approximation (BEMA). However, there is a Si–O–Si asymmetrical stretching mode for the annealed samples in the Fourier transform infrared (FTIR) spectroscopy spectrum (not shown here), indicating the additional interfacial growth. Therefore SE optical model should add an additional component of interfacial layer for the annealed ones to obtain a reasonably good fit. For ultrathin layers, the accurately determination of each fitting parameter is a difficult matter because of the correlation among them. In order to get the high accuracy, the thickness of the surface rough layer is set at a certain value from the atomic force microscopy (AFM) analysis. The surface rough layer thickness is listed in Table I, which is double the AFM root-mean-square (rms) values based on the reports of Song *et al.*[20]

Although the lowest χ^2 values (goodness of fit) are always larger than 1 (Table I), the fitted curves approach the experimental SE data very well (not shown here). Table I summarizes the SE fitting results. Since there is no observable Si–O–Si asymmetrical stretching mode in the FTIR spectrum for as-oxidized sample (not shown here), the interfacial layer is not considered. After annealing at 800 °C, there is only a little interfacial growth between ZrO_xN_y films and Si substrates, resulting in a 1.1 nm interfacial layer. While for ZrO_xN_y films annealed at 900 °C, there is a thick interfacial layer of 2.6 nm, indicating the significant interfacial growth consistent with the FTIR results. The SE fitting results indicate that our SE optical model adequately describe the measured data.

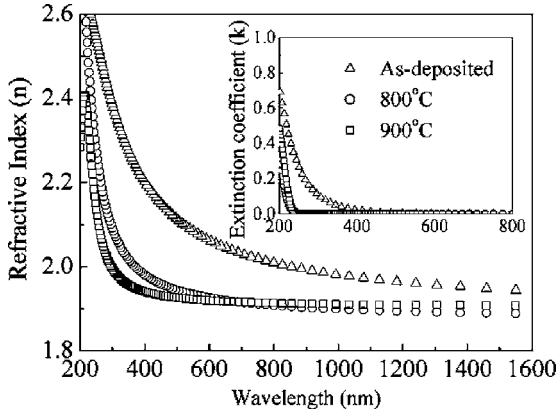

FIG. 2. Extracted refractive index and extinction coefficients for ZrO_xN_y films on Si. (△: as-oxidized, ○: 800 °C annealed, and □: 900 °C annealed.)

Figure 2 shows the refractive index n and extinction coefficient k of ZrO_xN_y films extracted from SE fitting results. It is clearly seen that the optical constants (n,k) are significantly affected by the additional high temperature annealing. For the as-oxidized ZrO_xN_y films, the optical constants (n,k) are much larger than the annealed ones. Since our XPS results indicate the reoxidization of Zr–N bonds in ZrO_xN_y matrix during *ex situ* annealing, we attribute the decrease in optical constants (n,k) to the reoxidization of Zr–N bonds and the annihilation of defects in ZrO_xN_y films caused by more incorporation of oxygen, consistent with the literature reports that the higher nitrogen concentration always results in the higher refractive index.[4,21] While increasing the annealing temperature further, there is no significant change in the optical constants, indirectly indicating the stabilized Zr–O–N bonds, consistent with the XPS results.

Optical absorption properties of ZrO_xN_y films are also studied, the absorption coefficients (α) are calculated using $\alpha=4\pi k/\lambda$ (where λ is the wavelength of a photon and k is the extinction coefficient) as a function of photon energy $(h\nu)$. Optical band gap energies E_g can be obtained by extrapolating the linear portion of the curves relating $(\alpha h\nu)^{1/2}$ and $h\nu$ to $(\alpha h\nu)^{1/2}=0$. The extracted optical band gap (E_g) shows a slight blueshift from 3.9 to 5.1 eV after the additional high temperature annealing in N_2/O_2 (shown in Table I). Our XPS results indicate that some nitrogen atoms substituted oxygen sites in the lattice of ZrO_2 crystal, which contributes to the low E_g values for as-oxidized ZrO_xN_y films because of the mixture between N_{2p} states and O_{2p} states.[22] After the additional high temperature annealing, the Zr–N bonds are fully oxidized, resulting in the blueshift in band gap energy. Since there are some N atoms in the ZrO_2 matrix for the annealed films, the band gap energies are still slightly lower than that of the stoichiometric ZrO_2 about 5.5 eV.[23]

XPS valence-band spectrum method can be used to determine the band alignment of dielectric/semiconductor heterostructure. Figure 3 shows the valence-band spectrum of 15 nm as-oxidized and 900 °C annealed ZrO_xN_y films and clean Si(100) substrates. The results indicate a valence-band offset of 2.27 and 2.78 eV for as-oxidized and 900 °C annealed ZrO_xN_y on Si, respectively. The existence of Zr–N bonds results in the lower valence-band edge for as-oxidized

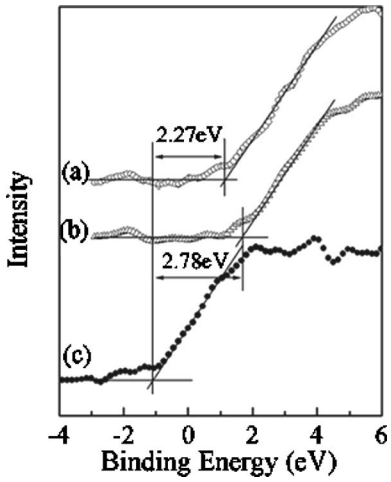

FIG. 3. Valence-band spectrum for ZrO_xN_y films on Si: (a) as oxidized, (b) 900 °C annealed, and (c) clean Si(100) substrates.

ZrO_xN_y. Similar effects are also observed for HfSiON system.[24] The slightly lower valence-band offset for 900 °C annealed ZrO_xN_y than that of the stociometric ZrO_2 about 2.95 eV (Ref. 25) is due to the formation of the stabilized Zr–O–N bonds. For as-oxidized ZrO_xN_y films, the conduction-band offset can be obtained by simply subtracting the valence-band offset and the energy gap of the substrate from the band gap of ZrO_xN_y,

$$\Delta E_C(\mathrm{ZrO}_x\mathrm{N}_y - \mathrm{Si}) = \mathrm{E}_g(\mathrm{ZrO}_x\mathrm{N}_y) - \Delta E_V(\mathrm{ZrO}_x\mathrm{N}_y - \mathrm{Si}) - E_g(\mathrm{Si}),$$

where $\Delta E_C(\mathrm{ZrO}_x\mathrm{N}_y - \mathrm{Si})$ is the conduction-band offset, $E_g(\mathrm{ZrO}_x\mathrm{N}_y)$ is the band gap of ZrO_xN_y, $\Delta E_V(\mathrm{ZrO}_x\mathrm{N}_y - \mathrm{Si})$ is the valence-band offset, and $E_g(\mathrm{Si})$ the band gap of Si substrate. Similarly, for $ZrO_xN_y/SiO_2/Si$ system, the conduction-band offset can also be derived,

$$\Delta E_C(\mathrm{ZrO}_x\mathrm{N}_y - \mathrm{SiO}_2) = E_g(\mathrm{SiO}_2) - \Delta E_V(\mathrm{SiO}_2 - \mathrm{Si}) + \Delta E_V(\mathrm{ZrO}_x\mathrm{N}_y - \mathrm{Si}) - E_g(\mathrm{ZrO}_x\mathrm{N}_y).$$

The energy-band lineup between SiO_2 and Si is obtained from the literature reports.[23] Using valence-band spectrum results and the SE measured band gap for ZrO_xN_y, the conduction-band offset is determined. Figure 4 shows the zero-field energy-band alignment for ZrO_xN_y/Si and $ZrO_xN_y/SiO_2/Si$ stacks. Since the conduction-band offset of SiO_2/Si is larger than that of ZrO_xN_y/Si, the formation of a thin SiO_2 interfacial layer will help to the improved interfacial properties. However, such layer should be carefully controlled.

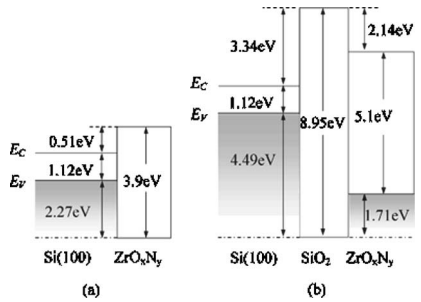

FIG. 4. Zero-field energy-band profile of ZrO_xN_y/Si system and $ZrO_xN_y/SiO_2/Si$ stacks for (a) as-oxidized and (b) 900 °C annealed ZrO_xN_y, respectively.

In summary, ZrO_xN_y films have been prepared by *ex situ* thermal oxidization of ZrN_x films on Si. XPS and SE results indicate that the bulk Zr–N bonds in as-oxidized ZrO_xN_y film are thermally unstable, while the Zr–O–N bonds are stable even at high temperature of 900 °C. The decrease in refractive index and extinction coefficients are attributed to the reoxidization of Zr–N bonds and the annihilation of defects in ZrO_xN_y films by more incorporation of oxygen. Optical absorption properties are also extracted. The slight blueshift in the absorption edge indicates the increased optical band gap. Interestingly, there is only a slight interfacial growth after annealing at 800 °C, while the significant interfacial growth occurs after annealing at 900 °C, indicating the stable interfacial properties up to 800 °C. Based on the valence-band spectrum results, the zero-field energy-band alignments for ZrO_xN_y/Si and $ZrO_xN_y/SiO_2/Si$ stacks are also extracted.

This work was supported by the National Key Project of Fundamental Research for Nanomaterials and Nanostructures (Grant No. 2005CB623603).

[1] G. D. Wilk, R. M. Wallace, and J. M. Anthony, J. Appl. Phys. **89**, 5243 (2001).
[2] M. L. Green, E. P. Gusev, R. Degraeve, and E. L. Garfunkel, J. Appl. Phys. **90**, 2057 (2001).
[3] T. S. Jeon, J. M. White, and D. L. Kwong, Appl. Phys. Lett. **78**, 368 (2001).
[4] S. Venkataraj, O. Kappertz, R. Jayavel, and M. Wuttig, J. Appl. Phys. **92**, 2461 (2002).
[5] D. Chi and P. C. Mclntyre, Appl. Phys. Lett. **85**, 4699 (2004).
[6] J. J. Yu and I. W. Boyd, Thin Solid Films **453/454**, 215 (2004).
[7] M. Zhu, P. Chen, R. K. Y. Fu, W. Liu, C. Lin, and P. K. Chu, Thin Solid Films **476**, 312 (2005).
[8] P. Victor and S. B. Krupanidhi, J. Phys. D **38**, 41 (2005).
[9] M. Houssa, M. Naili, C. Zhao, H. Bender, M. M. Heyns, and A. Stesmans, Semicond. Sci. Technol. **16**, 31 (2001).
[10] J. M. Howard, V. Craciun, V. Essary, and R. K. Singh, Appl. Phys. Lett. **81**, 3431 (2002).
[11] M. Couillard, M.-S. Lee, D. Landheer, X. Wu, and G. A. Botton, J. Electrochem. Soc. **152**, F101 (2005).
[12] A. P. Huang, R. K. Y. Fu, P. K. Chu, L. Wang, W. Y. Cheung, J. B. Xu, and S. P. Wong, J. Cryst. Growth **277**, 422 (2005).
[13] H. Jung, H. Yang, K. Im, and H. Hwang, Appl. Phys. Lett. **79**, 4408 (2001).
[14] H. Jung, K. Im, D. Yang, and H. Hwang, IEEE Electron Device Lett. **21**, 563 (2000).
[15] M. A. Quevedo-Lopez, M. El-Bouanani, M. J. Kim, B. E. Gnade, R. M. Wallace, M. R. Visokay, A. Li-Fatou, M. J. Bevan, and L. Colombo, Appl. Phys. Lett. **81**, 1609 (2002).
[16] C. S. Kang, H.-J. Cho, K. Onishi, R. Nieh, R. Choi, S. Gopalan, S. Krishnan, J. H. Han, and J. C. Lee, Appl. Phys. Lett. **81**, 2593 (2002).
[17] M. Lee, Z.-H. Lu, W.-T. Ng, D. Landheer, X. Wu, and S. Moisa, Appl. Phys. Lett. **83**, 2638 (2003).
[18] L. Pauling, *The Nature of the Chemical Bond* (Cornell University, Ithaca, New York, 1960).
[19] N. Martin, O. Banakh, A. M. E. Santo, S. Springer, R. Sanjinés, J. Takadoum, and F. Lévy, Appl. Surf. Sci. **185**, 123 (2001).
[20] Z. Song, B. R. Rogers, and N. D. Theodore, J. Vac. Sci. Technol. A **22**, 711 (2004).
[21] G. He, L. D. Zhang, G. H. Li, M. Liu, L. Q. Zhu, S. S. Pan, and Q. Fang, Appl. Phys. Lett. **86**, 232901 (2005).
[22] R. Asahi, T. Morikawa, T. Ohwaki, K. Aoki, and Y. Taga, Science **293**, 269 (2001).
[23] S. Miyazaki, J. Vac. Sci. Technol. B **19**, 2212 (2001).
[24] S. Sayan, Appl. Phys. Lett. **87**, 212905 (2006).
[25] S. J. Wang, A. C. H. Huan, Y. L. Foo, J. W. Chai, J. S. Pan, Q. Li, Y. F. Dong, Y. P. Feng, and C. K. Ong, Appl. Phys. Lett. **85**, 4418 (2004).